Non-planar 3D crack growth by the extended finite element and level sets. Part I: Mechanical model

Nicolas Moes, Anthony Gravouil, Ted Belytschko

Non-planar 3D crack growth by the extended finite element and level sets—Part I: Mechanical model

N. Moës[†], A. Gravouil[‡] and T. Belytschko[*,§]

Department of Mechanical Engineering, Northwestern University, 2145 Sheridan Road, Evanston, IL 60208, U.S.A.

A methodology for solving three-dimensional crack problems with geometries that are independent of the mesh is described. The method is based on the extended finite element method, in which the crack discontinuity is introduced as a Heaviside step function via a partition of unity. In addition, branch functions are introduced for all elements containing the crack front. The branch functions include asymptotic near-tip fields that improve the accuracy of the method. The crack geometry is described by two signed distance functions, which in turn can be defined by nodal values. Consequently, no explicit representation of the crack is needed. Examples for three-dimensional elastostatic problems are given and compared to analytic and benchmark solutions. The method is readily extendable to inelastic fracture problems.

KEY WORDS: fracture; cracks; discontinuous approximation; finite elements; level sets

1. INTRODUCTION

Three-dimensional fracture analysis of engineering problem by standard finite element methods is still quite difficult because of the need to construct a mesh which conforms to both the crack surfaces and the surfaces of the component. If the crack surface is not aligned with the element boundaries, the displacement discontinuity and the traction conditions on the crack surface cannot be treated by standard finite element methods. Furthermore, for standard elements, the mesh must be designed so that it is substantially more refined around the crack than in the remainder of the model. The difficulties are further amplified when considering the growth of cracks, because then the model must be remeshed in the vicinity of the crack. In addition to this, it must be borne in mind that initial cracks in many locations of the component must be considered for a complete engineering analysis.

*Correspondence to: Ted Belytschko, Department of Mechanical Engineering, Northwestern University, 2145 N. Sheridan, Evanston, IL 60208, U.S.A.
[†]Laboratoire de Mécanique et Matériaux, Ecole Centrale de Nantes, 1 Rue de la Noe, 44321 Nantes, France
[‡]Laboratoire de Mecanique des Solides, Institut National des Sciences Appliquées de Lyon, 34 Av. des Arts, 69621 Villeurbanne, France
[§]E-mail: tedbelytschko@northwestern.edu

This paper and a companion paper present further developments of the extended finite element method (X-FEM) for modelling cracks and crack growth. The extended finite element method alleviates much of the burden associated with mesh generation for objects with cracks by not requiring the finite elements to conform to the crack surface. Moreover, it provides a convenient way for incorporating near-tip asymptotic fields, so that good accuracy can be obtained for elastic fracture with relatively coarse meshes around the crack.

The essential idea in X-FEM is to use a displacement field approximation that can model an arbitrary discontinuity and the near-tip asymptotic crack fields. As a consequence it is often not necessary to modify the mesh to consider a specific crack; at most, moderate refinement must be introduced around the crack to achieve engineering accuracy in elastic fracture mechanics.

The methodology was first presented in References [1–3]. It was shown that discontinuous functions can be used to enrich finite element approximations via the partition of unity concept introduced by Melenk and Babuška [4]. The resulting approximation can treat cracks that are arbitrarily aligned in the finite element mesh with great accuracy. The concept was generalized in References [5, 6] which described the application of the concept to arbitrary discontinuities. Sukumar *et al.* [7] illustrated the potential of combining the extended finite element method with level sets by solving several problems involving inclusions and holes. In Reference [8] the extended finite element methodology was combined with a level set method to provide a general method for growing cracks. All of the preceding papers dealt with two-dimensional problems.

The first application of the extended finite element method to three-dimensional cracks was by Sukumar *et al.* [9], who solved several planar crack mode I problems and showed that the method compared well with analytical and benchmark solutions. Subsequently, Sukumar *et al.* [10] coupled the method with the fast marching method to solve several planar crack growth problems in three dimensions.

In this paper, the methodology is extended and modified so that it can handle arbitrary cracks in three dimensions. A key development that facilitates treatment of cracks in three dimensions is the description of crack geometry in terms of two signed distance functions. The displacement field is also described in terms of these signed distance functions. This enables us to construct a near-tip asymptotic field with a discontinuity that conforms to the crack even when it is curved or kinked near a tip. Furthermore, it eliminates the need for a surface model of the crack. As a consequence, no explicit representation of the crack is needed and the crack is entirely described by nodal data. Although the method described here will be for an elastic fracture, it is not limited to linear problems and can easily be extended to non-linear problems.

We cannot list references to all of the competing methods, but we list some recent papers in the following. The remeshing approach appears to be the most advanced for problems of an industrial type; recent accounts are given by Carter *et al.* [11] and Neto *et al.* [12]. Methods which rely on boundary element formulations combined with finite elements are given in References [13–15]. Duarte *et al.* [16] used the partition of unity concept with the visibility criterion to develop methods for dynamic three-dimensional crack growth. Three-dimensional dynamic crack growth by the element-free Galerkin method has been reported by Krysl and Belytschko [17]. The crack surface was represented by a set of triangular elements in 3D, which would be very awkward in a finite element method. The use of finite elements with embedded discontinuities also makes it possible to grow cracks in 2D without remeshing, see References [18, 19] for recent works on the topic.

The methodology for treating arbitrary three-dimensional cracks and their evolution by X-FEM are described in this and a companion paper. This paper focuses on the description of cracks in three dimensions in terms of level sets, the computation of the elastic solution and the stress intensity factors (SIFs), whereas the companion paper deals with the update of the level sets needed to model crack growth.

The outline of the paper is as follows. In Section 2, the methods for defining the crack geometry and the displacement fields are described. The governing equations are given in Section 3 as well as some implementation aspects. The SIF computations along the crack front are presented in Section 4. Section 5 reports some example calculations.

2. CRACK AND DISPLACEMENT FIELD DESCRIPTION

We consider a body Ω with an outer surface Γ and interior crack surfaces Γ_{cr}. The crack can be treated as a single surface or as two surfaces: Γ_{cr}^{+} and Γ_{cr}^{-}. In the latter case, the initial crack surfaces are considered coincident and the outward normals to the surface of the crack are denoted by $\mathbf{n}^{+}$ and $\mathbf{n}^{-}$, respectively.

Stolarska *et al.* [8] described a crack geometry in 2D by two signed distance functions. We also use two signed distance functions to describe a crack in 3D as shown in Figure 1. Note that the definition of the two level set functions is only needed in a neighbourhood of the crack. The signed distance function $\phi(\mathbf{x})$ defines the surface of the crack. It is given by

$$\phi(\mathbf{x}) = \min_{\bar{\mathbf{x}} \in \Gamma_{\text{cr}}^{\text{ext}}} \|\mathbf{x} - \bar{\mathbf{x}}\| \text{sign}(\mathbf{n}^{+} \cdot (\bar{\mathbf{x}} - \mathbf{x})) \tag{1}$$

where $\mathbf{x} = [x, y, z]$ and $\text{sign}(\cdot)$ is the sign function

$$\text{sign}(x) = \begin{cases} +1 & \text{if } x > 0 \\ -1 & \text{if } x < 0 \end{cases} \tag{2}$$

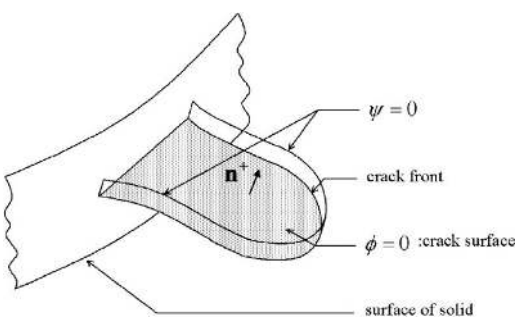

Figure 1. The two iso-zero level sets defining the crack location.

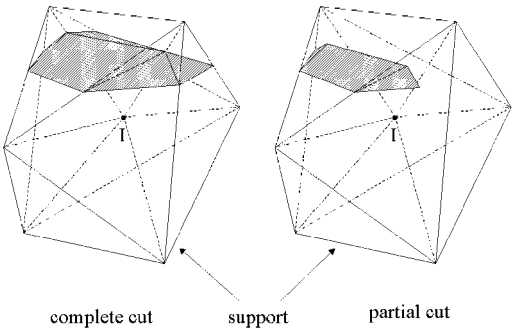

Figure 2. A node I whose support is completely and partially cut by the crack; the support is the volume of the elements connected to node I as shown.

We also need a smooth extension of the crack surface Γ_{cr}, denoted by Γ_{cr}^{ext}, which includes the entire crack surface, i.e. $\Gamma_{cr} \subset \Gamma_{cr}^{ext}$. The distance function (1) gives the shortest distance of any point $\mathbf{x}$ to the extension of the crack surface Γ_{cr}^{ext}. This corresponds to the orthogonal projection of $\mathbf{x}$ on Γ_{cr}^{ext}.

Since the crack surface Γ_{cr} is a bounded surface with a crack front, it is also necessary to define the crack front. This is accomplished by using a second signed distance function, $\psi(\mathbf{x})$, which is approximately orthogonal to $\phi(\mathbf{x})$ so that $\nabla\phi \cdot \nabla\psi \sim 0$. The intersection of the surfaces $\psi(\mathbf{x}) = 0$ and $\phi(\mathbf{x}) = 0$ gives the crack front; we define the sign of ψ so that $\phi(\mathbf{x}) = 0$, $\psi(\mathbf{x}) < 0$ gives the crack surface Γ_{cr}.

The signed distance functions in this paper are approximated by the same shape functions as the displacement field. Therefore, in the computations the signed distance functions are given by

$$\phi = \sum_I N_I(\mathbf{x})\phi_I \tag{3}$$

$$\psi = \sum_I N_I(\mathbf{x})\psi_I \tag{4}$$

where N_I are the finite element shape functions and ϕ_I and ψ_I are the nodal values of the distance function. This enables the crack shape to be described entirely in terms of nodal values. Of course, this is not necessary nor always most convenient. In some cases, it is easier to work with the functions themselves.

Since the shape functions are C^0, the representation of the crack surface and crack front is also C^0. In the studies reported here, four-node tetrahedra were used so the crack surface and crack front are piecewise linear. The method can be extended to higher order shape functions.

The displacement field $\mathbf{u}(\mathbf{x})$ for the body is decomposed into the continuous and discontinuous parts by

$$\mathbf{u} = \mathbf{u}_{cont} + \mathbf{u}_{dis} \tag{5}$$

where $\mathbf{u}_{cont}$ is continuous in Ω, whereas $\mathbf{u}_{dis}$ may have several surfaces of discontinuity in Ω. The locations of the discontinuities in $\mathbf{u}_{dis}$ are assumed to coincide with Γ_{cr}.

A standard finite element approximation is used for $\mathbf{u}_{cont}$, i.e.

$$\mathbf{u}_{cont} = \sum_{I \in \mathcal{N}} N_I(\mathbf{x})\mathbf{u}_I \tag{6}$$

where $\mathcal{N}$ is the set of all nodes in the mesh, N_I are the classical C^0 shape functions and $\mathbf{u}_I$ are displacement nodal degrees of freedom.

For the purpose of constructing the discontinuous field, the nodes are subdivided into three sets:

- $I \in \mathcal{N}_{cut}$: the set of nodes whose support (union of the elements connected to the node) are completely cut into two, i.e. bisected by the crack surface Γ_{cr}. An example of such a node is shown in Figure 2.
- $I \in \mathcal{N}_{branch}$: the set of nodes whose support are partially cut by the crack surface Γ_{cr}, see Figure 2 for an example of such a node.
- $I \in \mathcal{N} - \mathcal{N}_{cut} - \mathcal{N}_{cut}$: the remaining nodes.

The discontinuous displacement fields are given as follows:

$$\mathbf{u}_{\text{dis}} = \sum_{I \in \mathcal{N}_{\text{cut}}} N_I(\mathbf{x}) H(\phi(\mathbf{x})) \mathbf{a}_I + \sum_{I \in \mathcal{N}_{\text{branch}}} \sum_{\alpha} N_I(\mathbf{x}) B_\alpha(\phi(\mathbf{x}), \psi(\mathbf{x})) \mathbf{a}_{I\alpha} \tag{7}$$

In the above, $H(\cdot)$ if the Heaviside step function, $B_\alpha(.,.)$ are branch functions, and $\mathbf{a}_I$ and $\mathbf{a}_{I\alpha}$ are additional degrees of freedom for the displacement field. The branch functions are constructed in terms of the level set functions

$$[B_\alpha] = \left[\sqrt{r} \sin \frac{\theta}{2}, \sqrt{r} \cos \frac{\theta}{2}, \sqrt{r} \sin \frac{\theta}{2} \sin \theta, \sqrt{r} \cos \frac{\theta}{2} \sin \theta \right] \tag{8}$$

where

$$r = \sqrt{\phi^2 + \psi^2}, \quad \theta = \tan^{-1} \left(\frac{\phi}{\psi} \right) \tag{9}$$

Note that the branch functions have been expressed in terms of the level set functions. By expressing the branch functions B_α in terms of the level set functions, it is guaranteed that the discontinuity always corresponds to $\phi = 0$ and $\psi < 0$, i.e. to the surface of the crack. The resulting field will not contain the exact basis of the asymptotic near field, but it is more important to construct the discontinuity in the correct place than to match the exact near-tip asymptotic field.

Only the first of the functions in Equation (8) is discontinuous across $\phi = 0$. The others were added to improve the accuracy in elastic fracture problems. The above functions span the near-tip asymptotic solution for an elastic crack in two dimensions. In this study and previous studies [9] we have also found this basis to be quite accurate for three-dimensional cracks, although we have only considered smooth crack fronts.

This technique of adding asymptotic solutions through the a partition of unity in finite elements can be considered an asymptotic matching technique. The displacement fields in the other elements provide the far field, whereas the elements with the branch functions (8) provide the near field. The finite element procedure then matches these fields so that equilibrium is approximately satisfied.

3. GOVERNING EQUATIONS AND IMPLEMENTATION ASPECTS

We recall the equations of elastostatics under the assumptions of small strains and small displacements. We assume that the crack faces are traction-free although this is not an intrinsic limitation of the method. The outer boundary Γ of the domain Ω is decomposed into Γ_t on which tractions $\bar{\mathbf{t}}$ are imposed and Γ_u on which displacements $\bar{\mathbf{u}}$ are imposed. The Cauchy stress tensor field $\boldsymbol{\sigma}$ must satisfy the equilibrium conditions

$$\boldsymbol{\nabla} \cdot \boldsymbol{\sigma} = 0 \quad \text{on } \Omega, \qquad \boldsymbol{\sigma} \cdot \mathbf{n} = \bar{\mathbf{t}} \quad \text{on } \Gamma_t \tag{10}$$

$$\boldsymbol{\sigma} \cdot \mathbf{n}^+ = 0 \quad \text{on } \Gamma_{\text{cr}}^+, \qquad \boldsymbol{\sigma} \cdot \mathbf{n}^- = 0 \quad \text{on } \Gamma_{\text{cr}}^- \tag{11}$$

The kinematic equations involve the strain–displacement relationship and the displacement boundary condition. Under the assumptions of small strains and displacements, they are

$$\boldsymbol{\varepsilon} = \tfrac{1}{2}(\nabla \mathbf{u} + (\boldsymbol{\nabla} \mathbf{u})^{\mathrm{t}}) \equiv \boldsymbol{\varepsilon}(\mathbf{u}) \quad \text{on } \Omega, \quad \mathbf{u} = \bar{\mathbf{u}} \quad \text{on } \Gamma_u$$

The constitutive law is linear in the examples solved here, so

$$\boldsymbol{\sigma} = \mathbf{C} : \boldsymbol{\varepsilon} \quad \text{on } \Omega \tag{12}$$

where $\mathbf{C}$ is Hooke's tensor.

The strong form of the equilibrium equations and associated boundary condition is equivalent to the following weak form [1]: find $\mathbf{u} \in \mathscr{U}$ such that

$$\int_{\Omega} \boldsymbol{\varepsilon}(\mathbf{u}) : \mathbf{C} : \boldsymbol{\varepsilon}(\mathbf{v}) \, \mathrm{d}\mathbf{x} = \int_{\Gamma_t} \bar{\mathbf{t}} \cdot \mathbf{v} \, \mathrm{d}\Gamma_t \quad \forall \mathbf{v} \in \mathscr{U}_0 \tag{13}$$

where $\mathscr{U}$ is the set of kinematically admissible displacement fields:

$$\mathscr{U} = \{\mathbf{u} \in \mathscr{V} \mid \mathbf{u} = \bar{\mathbf{u}} \text{ on } \Gamma_u \ \mathbf{u} \text{ discontinuous on } \Gamma_{\mathrm{cr}}\} \tag{14}$$

and $\mathscr{U}_0$ is the set of kinematically admissible displacement fields for zero prescribed displacements:

$$\mathscr{U}_0 = \{\mathbf{v} \in \mathscr{V} \mid \mathbf{v} = \mathbf{0} \text{ on } \Gamma_u \ \mathbf{v} \text{ discontinuous on } \Gamma_{\mathrm{cr}}\} \tag{15}$$

The exact mathematical nature of the space $\mathscr{V}$ is related to the regularity of the solution. It is important to note that $\mathscr{U}$ and $\mathscr{U}_0$ allows discontinuous displacement fields across Γ_{cr}. The introduction of the discrete finite displacement field (5)–(7) into the weak form (13) yields the linear system of equations. The displacement fields given in the previous section are used for both $\mathbf{u}$ and $\mathbf{v}$. Explicit forms of the stiffness matrix can be found in Reference [9].

In the elements cut by the crack, the displacement field is discontinuous and some special care is needed when performing the integration appearing in Equation (13). We use a technique introduced in Reference [2] for 2D and in Reference [9] for 3D which consists of separately integrating on each side of the crack using a decomposition of the elements into sub-tetrahedrons. For the elements enriched by the branch function, the displacement fields involve non-polynomial functions (the square root and trigonometric functions). We use a 15-point integration rule on these elements (or sub-tetrahedrons if the element is cut by the crack). A single Gauss point is used in all other four-node tetrahedral elements.

In Section 2, we have defined the nodes that are enriched by the Heaviside function as the set of nodes whose support is completely cut by the crack. A direct use of this criterion may lead to an ill-conditioned stiffness matrix. Consider Figure 3(a) which illustrates a crack cutting across finite elements. Nodes a and b are enriched since their support is completely cut by the crack whereas nodes c and d are not enriched since their support is not cut by the crack. In Figure 3(b), a direct application of the support criterion leads to the enrichment of the nodes c and d. The regular and enriched shape functions at these nodes will only differ in the very thin band of width ε, leading to ill-conditioning of the system matrix because of near-linear dependence of the resulting basis functions. We therefore enrich a node only if the volume of the subdomains generated by a cut exceeds a tolerance. This criterion was introduced in Reference [2].

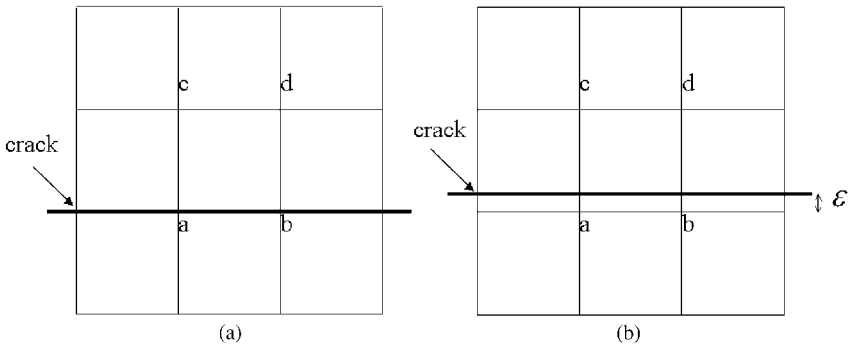

Figure 3. Effects of cracks near edges: (a) crack aligned with a mesh. The nodes a and b are enriched and the nodes c and d are not enriched; and (b) crack almost aligned with a mesh. The nodes c and d should not be enriched to avoid ill-conditioning.

Another strategy that we shall adopt in this paper is to avoid the situation depicted in Figure 3(b). Before deciding whether a node is enriched, we slightly modify the level set functions as follows. If the level set changes sign on an edge, we determine where it vanishes. If it vanishes very close to one of the nodes of the edge, we set the level set to be zero at that node.

More precisely, an edge with nodes at $\mathbf{x}_a$ and $\mathbf{x}_b$ is a line given by

$$\mathbf{x} = (1 - r)\mathbf{x}_a + r\mathbf{x}_b, \quad r \in [0, 1] \tag{16}$$

Let f_a and f_b be the level set function values at the two nodes. If the level set f changes sign along the edge, it vanishes at $r_0 = f_a/(f_a - f_b)$. If $r_0 < \text{tol}$ we set the level set function to zero at node a or if $1 - r_0 < \text{tol}$, we set the level set function to zero at node b. A tolerance of 10^{-2} is used in the numerical examples. This procedure avoids the situation shown in Figure 3(b) and the geometrical decomposition of the element cut by the crack (for integration purpose) into sub-tetrahedra then does not require any tolerance parameters.

In our implementation, we use a mesh database called Algorithm Oriented Mesh Database (AOMD) [20, 21]. This database is very flexible and considerably simplifies operations like finding the set of nodes whose supports are cut by the crack.

4. STRESS INTENSITY FACTOR COMPUTATION

A domain integral is used to compute the energy release rate at any sample point on the front and a so-called interaction integral is used to separately compute the three stress intensity factors. A general discussion of crack-tip contour integrals and their associated domain integral representations is given in Reference [22]. The specific interaction integral we use was introduced in Reference [23] for planar cracks with curved fronts and in Reference [24] for non-planar cracks. It involves the use of auxiliary fields corresponding to the crack-tip fields in plane strain and anti-plane motion. The use of domain energy integrals in the finite element framework provides high accuracy while keeping the implementation rather simple as shown in Reference [25].

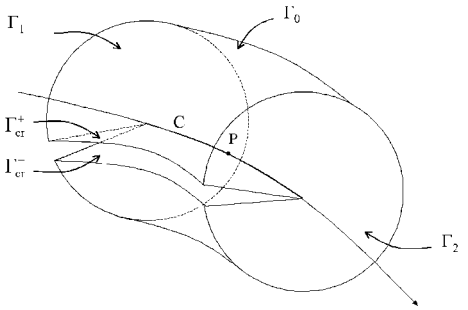

Figure 4. Notation for the J-domain integral computation.

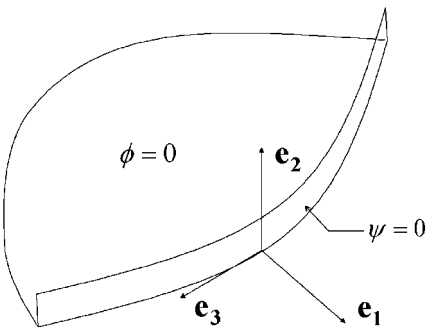

Figure 5. Local axis on the front obtained from the level set crack description through formula (17).

Consider a point $\mathbf{p}$ located on the crack front as shown in Figure 4 for which we would like to compute the stress intensity factors K_1, K_2 and K_3. A volume V is constructed around the point of interest $\mathbf{p}$. It intercepts the arc C of the crack front and consists of the crack surfaces Γ_{cr}^+, Γ_{cr}^- and the three surfaces Γ_0, Γ_1, Γ_2.

Using the level set crack representation, we define at any point inside the domain V a local basis $(\mathbf{e}_1, \mathbf{e}_2, \mathbf{e}_3)$. The gradient of the level sets are good candidates for such a basis and were already used by Sukumar *et al.* [10] to define the local basis on the crack front. However, since the level sets are linear over each element, their gradients are discontinuous from element to element. We define the vector basis $(\mathbf{e}_1, \mathbf{e}_2, \mathbf{e}_3)$ by a smoothed gradient of the level set. Let $\mathbf{x}$ by an arbitrary point inside the element $\mathbf{e}$ whose nodes are in the set $\mathcal{N}_e$. The basis vectors at $\mathbf{x}$ are defined by

$$\mathbf{e}_1 = \sum_{I \in \mathcal{N}_e} N_I(\mathbf{x}) \nabla \psi|_I, \quad \mathbf{e}_2 = \sum_{i \in \mathcal{N}_e} N_I(\mathbf{x}) \nabla \phi|_I, \quad \mathbf{e}_3 = \mathbf{e}_1 \times \mathbf{e}_2 \tag{17}$$

where the nodal gradient at node I, $\nabla \cdot|_I$, is the average of the gradients of the element connected to node I. Figure 5 shows the local basis vectors for a point located on the front.

All vectors and tensors are expressed in this varying system of co-ordinates (17) similar to corotational co-ordinates [26]. For instance, the Eshelby tensor is given by

$$\hat{P}_{ij} = w\delta_{ij} - \hat{\sigma}_{kj}\hat{u}_{k,i} \tag{18}$$

where $w = \frac{1}{2}\sigma_{kl}\varepsilon_{kl}$ is the elastic energy density and a superposed hat refers to components in the local $(\mathbf{e}_1, \mathbf{e}_2, \mathbf{e}_3)$ basis.

In the domain V, we define a virtual velocity field $\mathbf{q}$ as

$$\mathbf{q} = \alpha \mathbf{e}_1; \quad \alpha(\mathbf{p}) = 1 \quad \text{and} \quad \alpha(\mathbf{x}) = 0 \quad \text{for } \mathbf{x} \in \Gamma_0 \cup \Gamma_1 \cup \Gamma_2 \tag{19}$$

where α is a scalar field taking a value of 1 at $\mathbf{p}$ and 0 on $\Gamma_0 \cup \Gamma_1 \cup \Gamma_2$. The $\mathbf{q}$ field is tangent to the crack faces on the crack and on the front, see Figure 6(b).

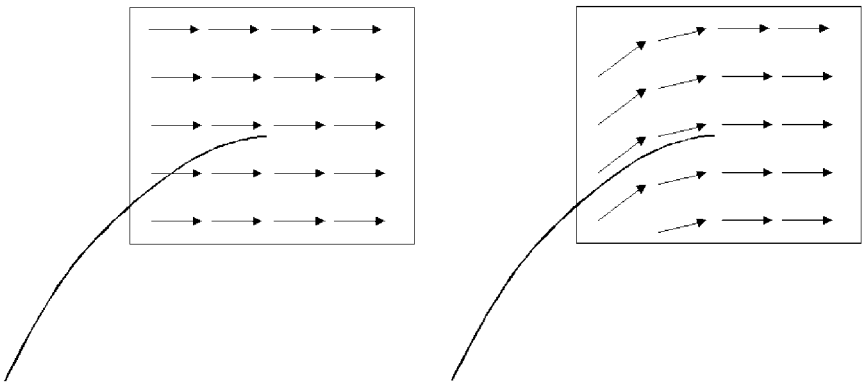

Figure 6. (a) A virtual velocity field with fixed orientation; and (b) respecting the crack geometry.

The J-domain integral is given by

$$J = \int_{\Gamma_{cr}^{+} \cup \Gamma_{cr}^{-}} \hat{q}_i \hat{P}_{ij} \hat{n}_j \, d\Gamma - \int_V \hat{q}_{i,j} \hat{P}_{ij} \, dV \tag{20}$$

where **n** denotes the outward normal to the domain V. In the following, we drop the superposed hats but note that all computations are made in local basis. If the crack faces are free of tractions, the crack surface integral vanishes, so

$$J = - \int_V q_{i,j} P_{ij} \tag{21}$$

The boundary term on the crack faces vanishes by construction, the virtual velocity **q** is tangent to the crack faces ($n_j w q_j = 0$) and the crack surfaces are free of tractions ($\sigma_{ij} n_j = 0$).

Note that our choice for the **q** field is original. Usually, see for instance [24], the orientation of the virtual crack extension vector **q** is fixed over the entire domain V. In that case, the crack surface integral in Equation (20) may not be dropped. The ability of the level set crack representation to provide a good local system of co-ordinates should be noted.

The J-domain integral (20) measures the strength of the singularity around the arc C. More precisely, it is the power released if the crack front were to advance under the virtual crack extension velocity **q** (whose magnitude is α):

$$J = \int_C \alpha G \, dC \tag{22}$$

where G is the energy release rate:

$$G = \frac{(1 - \nu^2)}{E} (K_1^2 + K_2^2) + \frac{1}{2\mu} K_3^2 \tag{23}$$

In order to extract the three modes, we use the interaction integral concept which may be summarized as follows. The J-domain integral (20) is a function of the stress, strain and

displacement fields around the crack front C, namely $J = J(\boldsymbol{\sigma}, \boldsymbol{\varepsilon}, \mathbf{u})$. If we add to the exact fields the auxiliary fields, $(\boldsymbol{\sigma}^{\text{aux}}, \boldsymbol{\varepsilon}^{\text{aux}}, \mathbf{u}^{\text{aux}})$, we obtain

$$J(\boldsymbol{\sigma} + \boldsymbol{\sigma}^{\text{aux}}, \boldsymbol{\varepsilon} + \boldsymbol{\varepsilon}^{\text{aux}}, \mathbf{u} + \mathbf{u}^{\text{aux}}) = J(\boldsymbol{\sigma}, \boldsymbol{\varepsilon}, \mathbf{u}) + J(\boldsymbol{\sigma}^{\text{aux}}, \boldsymbol{\varepsilon}^{\text{aux}}, \mathbf{u}^{\text{aux}}) + I \tag{24}$$

where the interaction integral I is given by

$$I = \int_{\Gamma_{\text{cr}}^{+} \cup \Gamma_{\text{cr}}^{-}} q_i P_{ij}^{\text{aux}} n_j \, \mathrm{d}\Gamma - \int_V q_{i,j} P_{ij}^{\text{aux}} \, \mathrm{d}V - \int_V q_i P_{ij,j}^{\text{aux}} \, \mathrm{d}V \tag{25}$$

and

$$P_{ij}^{\text{aux}} = \tfrac{1}{2} \sigma_{kl} \varepsilon_{kl}^{\text{aux}} \delta_{ij} + \tfrac{1}{2} \sigma_{kl}^{\text{aux}} \varepsilon_{kl} \delta_{ij} - \sigma_{kj}^{\text{aux}} u_{k,i} - \sigma_{kj} u_{k,i}^{\text{aux}} \tag{26}$$

To be precise, the expression for J used in Equation (24) is not given by Equation (20) but by

$$J = \int_{\Gamma_{\text{cr}}^{+} \cup \Gamma_{\text{cr}}^{-}} q_i P_{ij} n_j \, \mathrm{d}\Gamma - \int_V (q_i P_{ij})_{,j} \, \mathrm{d}V \tag{27}$$

The latter has the advantage of being domain independent, and so is I, even though the auxiliary fields do not satisfy the governing equations. Indeed, the auxiliary fields correspond to the plane strain and anti-plane crack-tip fields and thus will not satisfy the governing equation for a non-planar or even for a plane crack with a curved front. That is they cannot at the same time satisfy equilibrium, compatibility and Hooke's law. We shall follow Gosz and Moran [24] and enforce the constitutive law, i.e. auxiliary strains are given in terms of auxiliary stresses through Hooke's law and not in terms of displacement gradients. The interaction integral is then

$$I = -\int_V q_{i,j} (\sigma_{kl} \varepsilon_{kl}^{\text{aux}} \delta_{ij} - \sigma_{kj}^{\text{aux}} u_{k,i} - \sigma_{kj} u_{k,i}^{\text{aux}}) \, \mathrm{d}V - \int_V q_i (\sigma_{kl,i}^{\text{aux}} \varepsilon_{kl} \delta_{ij} - \sigma_{kl} u_{k,li}^{\text{aux}} - \sigma_{kl,l}^{\text{aux}} u_{k,i}) \, \mathrm{d}V \tag{28}$$

Again, the crack surface integral are eliminated by assuming traction-free crack faces and using the fact that the auxiliary stress fields are expressed in the level set co-ordinates. Therefore, $\sigma_{ij}^{\text{aux}} n_j = 0$, even though the crack is not necessarily planar.

The interaction integral is given by

$$I = \int_C \alpha G^{\text{aux}} \, \mathrm{d}C \tag{29}$$

where

$$G^{\text{aux}} = \frac{2(1 - \nu^2)}{E} (K_1 K_1^{\text{aux}} + K_2 K_2^{\text{aux}}) + \frac{1}{\mu} K_3 K_3^{\text{aux}} \tag{30}$$

Here, in Equation (30), K_1^{aux}, K_2^{aux} and K_3^{aux} are the stress intensity factors associated with the auxiliary fields and K_1, K_2 and K_3 are the stress intensity factors associated with the actual fields. The process of evaluating the mixed-mode stress intensity factors involves making a judicious choice of the auxiliary stress intensity factors, and then evaluating the interaction

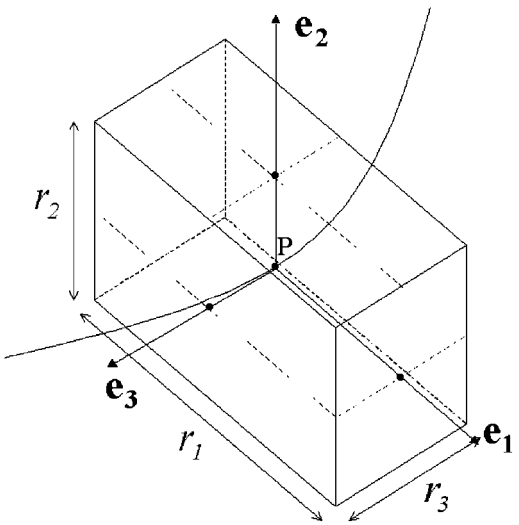

Figure 7. The domain used to extract the stress intensity factors at a point **p**.

integral (28). For example, substituting $K_1^{\text{aux}} = 1$, and $K_2^{\text{aux}} = K_3^{\text{aux}} = 0$ into Equations (29) and (30) yields

$$I = \frac{2(1-\nu^2)}{E} \int_C \alpha K_1 \, \mathrm{d}C \tag{31}$$

from which Gosz *et al.* [23] deduce the approximate expression for K_1

$$K_1 = \frac{E}{2(1-\nu^2)} \frac{I}{\int_C \alpha \, \mathrm{d}C} = \frac{E}{(1-\nu^2)} \frac{I}{\text{meas}(C)} \tag{32}$$

Similarly, we can compute the energy release rate by

$$G = \frac{E}{(1-\nu^2)} \frac{J}{\text{meas}(C)} \tag{33}$$

In the construction of the domain V and the α scalar field, we follow Sukumar *et al.* [9]. The domain V is a parallelipiped as shown in Figure 7. It is decomposed into a number of cells ($2 \times 2 \times 2$ in this paper) over which integration is performed. We use $6 \times 6 \times 6$ quadrature rule in each integration cell. When the crack front is close to the surface of the body, some integration points may be located outside the body. They are discarded from the integration procedure.

Finally, we need to discuss how the crack front is built from two level set functions ϕ and ψ. We assume that the mesh is composed of tetrahedral elements. If hexahedra or prisms are present, we suggest breaking them into tetrahedra (for the level set representation only, the displacement field may still use the hexahedral- or prism-based interpolation).

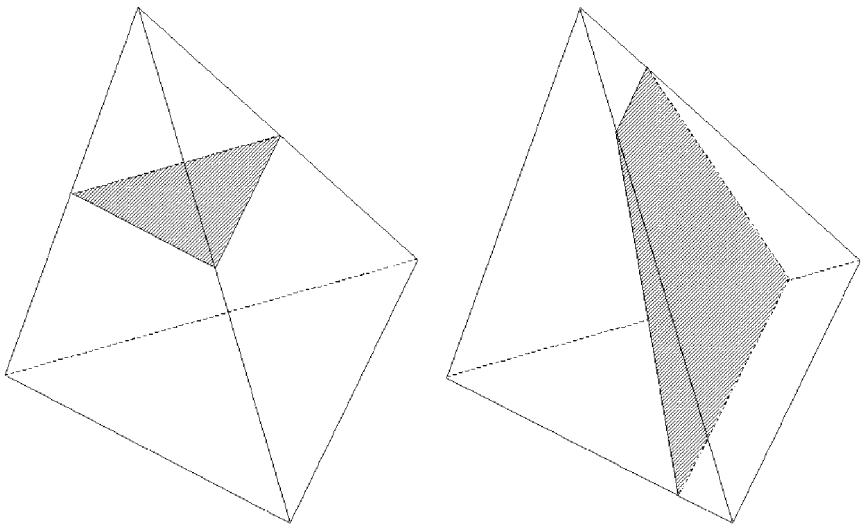

Figure 8. (a) The iso-zero level set inside a tetrahedron is either a triangle; and (b) a quadrilateral.

We loop over the elements in the mesh (or more precisely the narrow band). If ϕ changes sign on an element, we find the iso-zero location of the level set inside this element. It is either a triangle or a quadrilateral as shown in Figure 8. If it is a quadrilateral, it is split into two triangles. The union of these triangles form a surface mesh. To each node of this surface mesh we assign the value of the ψ level set. The location of the crack front is then the iso-zero ψ level set on the surface mesh and consists of a set of segments.

5. NUMERICAL EXPERIMENTS

The stress intensity factors along the crack front are of primary importance in determining the orientation and magnitude of the crack front velocity. The companion paper [27] will describe how this information is used to model fatigue crack growth.

In this section, we examine how accurately we can compute the SIFs along the crack front using X-FEM and the level set representation of the crack described in the previous sections. Two benchmark problems are considered: a lens-shaped crack and an inclined elliptical crack. Finally, a mechanical part containing a semi-circular crack is analysed.

5.1. A lens-shaped crack

The geometry of the lens-shaped crack is shown in Figure 9. The crack geometry can be characterized by the radius R and the angle α. Martynenko and Ulitko [28] determined the analytical solution for this crack in an infinite solid subjected to a uniform stress field. Gosz and Moran [24] used this reference solution as a benchmark. The crack is embedded in a cube with sides $2h$; we set h so that boundary effects are small. In the present example, the geometric parameters were chosen such that $h/R = 5$ and $\alpha = \pi/4$. Young's modulus and Poisson's ratio were taken to be $E = 68.9$ GPa and $\nu = 0.22$.

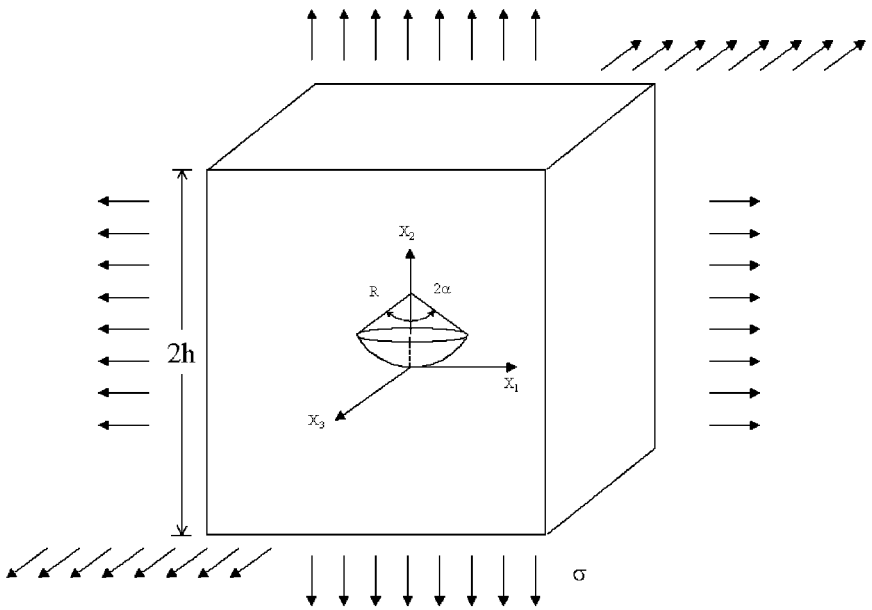

Figure 9. The problem of a lens-shaped crack in a cube subjected to hydrostatic tension.

For this crack geometry and material parameters, the analytical stress intensity factors are given in Reference [24]:

$$K_1^{\text{ref}} = 0.877\frac{2}{\pi}\sigma\sqrt{\pi a}, \quad K_2^{\text{ref}} = 0.235\frac{2}{\pi}\sigma\sqrt{\pi a} \tag{34}$$

where $a = R\cos(\alpha)$ and σ is the magnitude of the hydrostatic tensile loading.

The computational model is an unstructured tetrahedral mesh refined so that element size in the vicinity of the crack is about 4 per cent of elements near the boundary. The characteristic element size close to the front is $R/20$. The number of degrees of freedom is 145 000. The stress intensity factors are computed at 10 points along the crack front. The box size for the stress intensity computation is $r_1 = r_2 = R/4$, $r_3 = r_1/2$, see Figure 7. Figure 10 compares the stress intensity factors computed to the analytical stress intensity factors. Maximum errors are about 2 per cent for K_1 and 10 per cent for K_2. To put this in perspective, Gosz and Moran [24] used a mesh matching the crack surface in which the characteristic length of the smallest elements near the tip is $R/500$ (against $R/20$ in our computation). They achieved somewhat better accuracy with a maximum error of 0.3 per cent in K_1 and 5 per cent in K_2.

5.2. An inclined elliptical crack

The second problem is an inclined elliptical crack under tension. This problem was considered as a benchmark by Singh *et al.* [29]. In contrast to the previous problem, this crack geometry has a varying curvature along the crack front leading to varying stress intensity factors. The analytical solution of an elliptical crack embedded in an infinite domain was determined by Kassir and Sih [30].

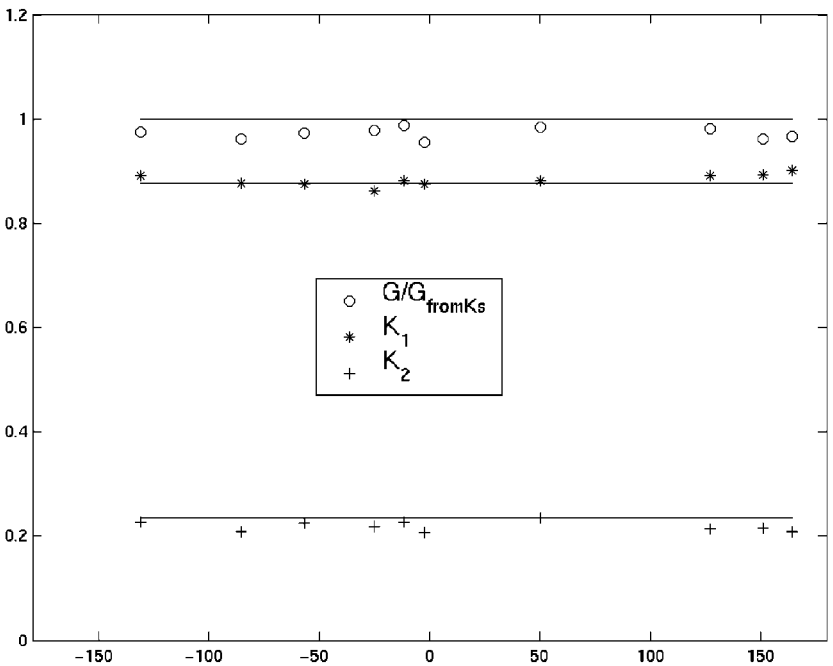

Figure 10. The computed stress intensity factors ($K_1 = *$, $K_2 = +$) compared to the exact stress intensity factors (solid lines). The exact and computed stress intensity factors were normalized by $(2/\pi)\sigma\sqrt{\pi a}$. The ratio between the energy release rate G computed by the domain integral (33) and by Equation (23) is as shown. The abscissa indicates the location on the front in degrees (the crack front is circular).

In the computations, the crack is placed in a cube of width h under tension along the Z-axis, see Figure 11. The major ellipse axis of length a is along X and the minor axis of length $b = a/2$ is the bisector of the XY quadrant, i.e. the crack is inclined at 45° with respect to the loading. The dimensions are chosen so that boundary effects are small $h/a = 10$. Poisson's ratio is 0.3 and Young's modulus 1.

Figure 13 shows a comparison of the exact and numerical stress intensity factors. The abscissa is the angle θ (in degrees) defined in Figure 12.

The number of degrees of freedom in the system was 130 000 and the characteristic element size along the front was only $a/10$. The results are, however, quite accurate.

5.3. Industrial part

To show the applicability of the method to more complicated shapes, we consider the mechanical part shown in Figure 14 taken from the `gmsh` mesher web page [31]. The loading is shown in Figure 15 and consists of an applied pressure of 2 MPa on two opposite sectors of the inner surface of the hole. The crack is semi-circular with a radius of 0.03, and its centre is located on the part mid-plane as shown in Figure 15. The mesh used is shown in Figure 16. It does not conform to the crack and has been refined in the crack area. The rigid modes of the part are removed by setting to zero the appropriate displacement components at three different points. Young's modulus is 200 MPa and Poisson's ratio is 0.3.

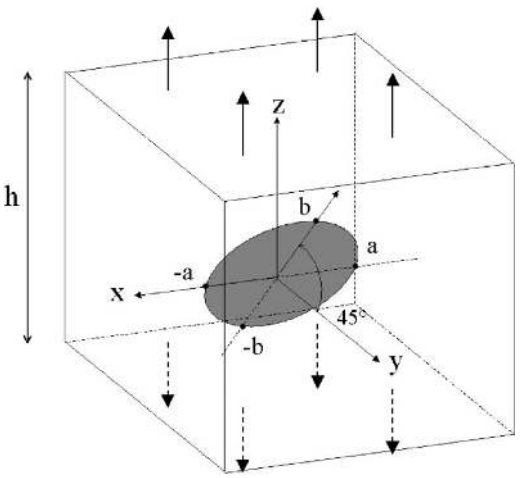

Figure 11. The problem of an inclined elliptical crack under tension.

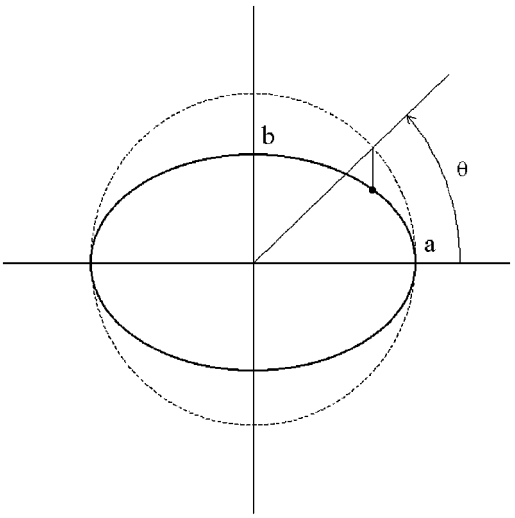

Figure 12. Definition of the angular position for an elliptical crack.

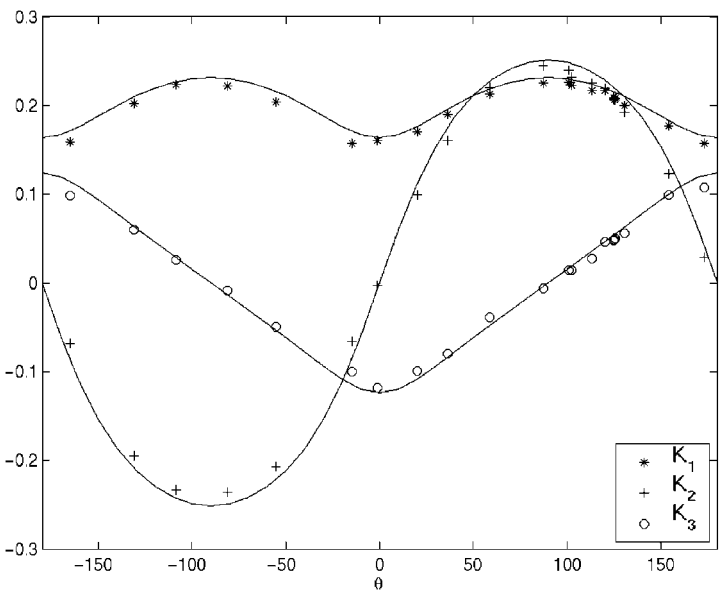

Figure 13. The exact (solid lines) and computed (symbols) stress intensity factors for the elliptical crack problem.

The stress intensity factors are computed at the mid-point of each segment on the front following the strategy described in Section 4. The box size for the stress intensity computation is $r_1 = r_2 = 2l$, $r_3 = r_1/2$, where l is the characteristic size of the elements near the point where the stress intensity factors are evaluated.

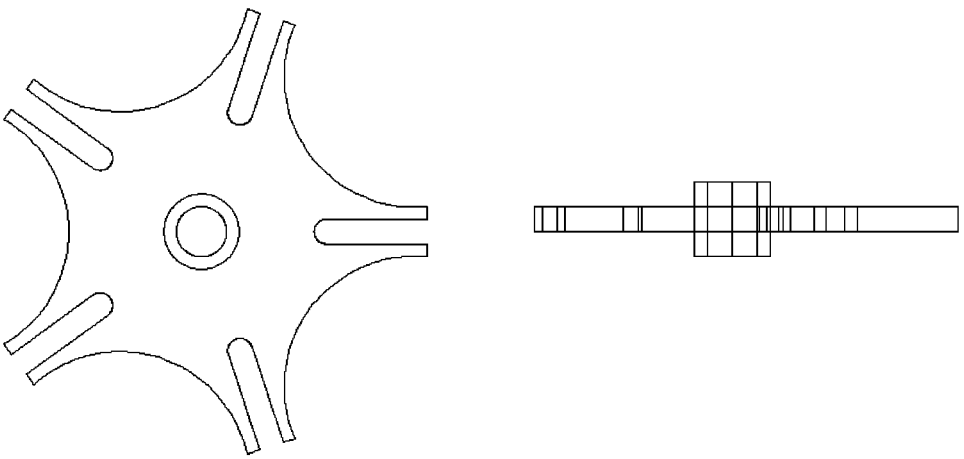

Figure 14. Face and side view of a mechanical part (Maltese cross).

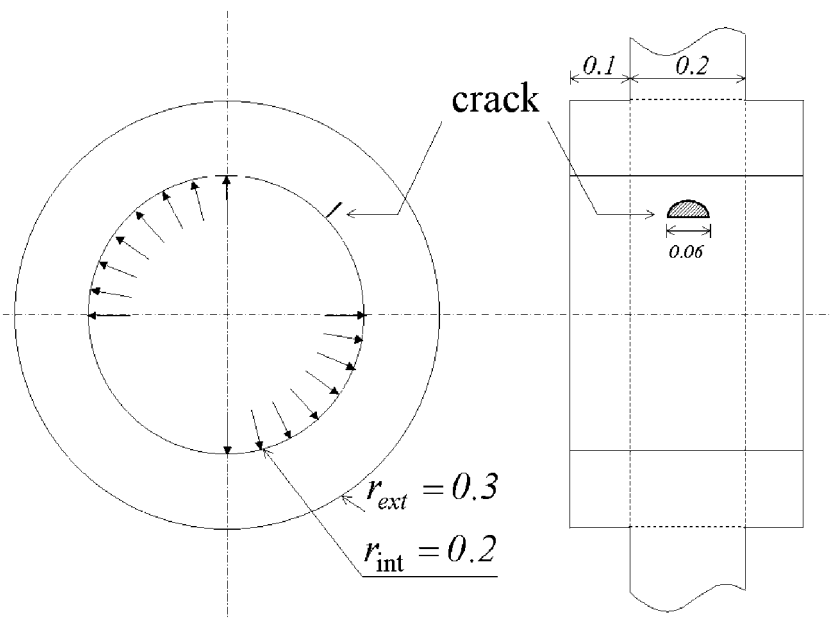

Figure 15. Zoom on the part: face and side view to show the location of the semi-circular crack and the loading.

Due to the symmetry in the problem (the crack plane is a plane of symmetry), the crack is in mode I and indeed the numerical modes II and III stress intensity factors are at least 50 times smaller than the mode I stress intensity factor. The energy release rate along the crack front is shown in Figure 17.

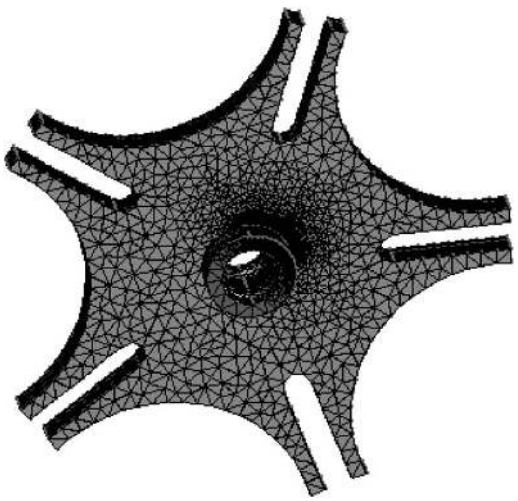

Figure 16. The mesh used for the analysis of the mechanical part: 161 925 tetrahedral elements.

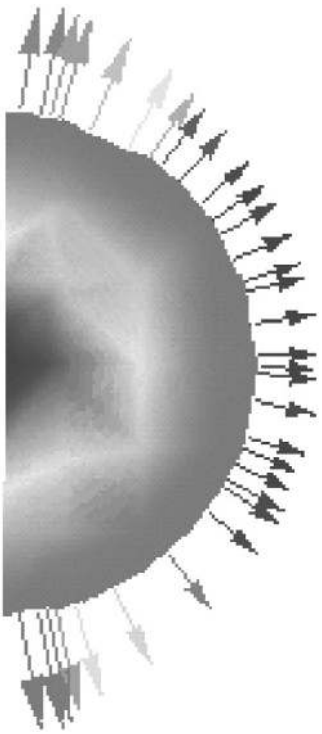

Figure 17. Energy release rate along the semi-circular crack front, shown as the magnitude of the vector normal to the front.

6. CONCLUSIONS

A method has been developed for the analysis of arbitrary cracks in three-dimensional bodies. The method combines the extended finite element method, which constructs arbitrary discontinuities through a discontinuous partition of unity with level set methods. The two methodologies are tightly integrated: the discontinuous partition of unity approximation is formulated in terms of the level sets. The advantage of the method is that the element topology need not conform to the surfaces of the cracks. The crack can cut any element arbitrarily and the crack front can pass through an element. For elasto-static fracture problems, the near-tip asymptotic fields have been embedded so that good accuracy is achieved with coarse meshes.

A method for stress intensity factor calculation has been developed that takes advantage of beneficial properties of variables in the level set co-ordinates. This streamlines the stress intensity factor computation and allows it to account for the curvature of the crack surface near the crack front.

In contrast to remeshing methods, the crack can be altered or grown by simply changing the level sets. This facilitates engineering analysis, where a thorough analysis of a structure requires consideration of many possible cracks. Ultimately, it is likely that design will entail

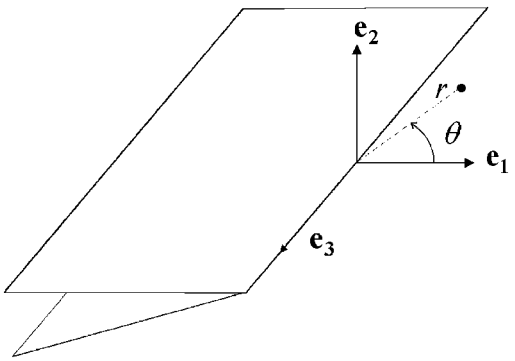

Figure 18. Coordinate system for the definition of the auxiliary fields.

antioptimization of the component: finding the location of a crack of given size (i.e. one not detectable by non-destructive evaluation) that minimizes the design load. Such engineering approaches will require highly automated methods for simulating crack growth that do not entail remeshing.

APPENDIX A: THE AUXILIARY FIELDS

The auxiliary stresses are

$$\sigma_{11}^{\text{aux}} = \frac{1}{\sqrt{2\pi r}} \left\{ K_1^{\text{aux}} \cos\frac{\theta}{2}\left[1 - \sin\frac{\theta}{2}\sin\frac{3\theta}{2}\right] - K_2^{\text{aux}} \sin\frac{\theta}{2}\left[2 + \cos\frac{\theta}{2}\cos\frac{3\theta}{2}\right]\right\} \tag{A1}$$

$$\sigma_{22}^{\text{aux}} = \frac{1}{\sqrt{2\pi r}} \left\{ K_1^{\text{aux}} \cos\frac{\theta}{2}\left[1 + \sin\frac{\theta}{2}\sin\frac{3\theta}{2}\right] + K_2^{\text{aux}} \sin\frac{\theta}{2}\cos\frac{\theta}{2}\cos\frac{3\theta}{2}\right\} \tag{A2}$$

$$\sigma_{12}^{\text{aux}} = \frac{1}{\sqrt{2\pi r}} \left\{ K_1^{\text{aux}} \sin\frac{\theta}{2}\cos\frac{\theta}{2}\cos\frac{3\theta}{2} + K_2^{\text{aux}} \cos\frac{\theta}{2}\left[1 - \sin\frac{\theta}{2}\sin\frac{3\theta}{2}\right]\right\} \tag{A3}$$

$$\sigma_{23}^{\text{aux}} = \frac{K_3^{\text{aux}}}{\sqrt{2\pi r}}\cos\frac{\theta}{2}, \quad \sigma_{13}^{\text{aux}} = -\frac{K_3^{\text{aux}}}{\sqrt{2\pi r}}\sin\frac{\theta}{2}, \quad \sigma_{33}^{\text{aux}} = \nu(\sigma_{11}^{\text{aux}} + \sigma_{22}^{\text{aux}}) \tag{A4}$$

whereas the auxiliary displacement fields are

$$u_1^{\text{aux}} = \frac{1}{2\mu}\sqrt{\frac{r}{2\pi}} \left\{ K_1^{\text{aux}} \cos\frac{\theta}{2}(\kappa - \cos\theta) + K_2^{\text{aux}} \sin\frac{\theta}{2}(\kappa + 2 + \cos\theta)\right\} \tag{A5}$$

$$u_2^{\text{aux}} = \frac{1}{2\mu}\sqrt{\frac{r}{2\pi}} \left\{ K_1^{\text{aux}} \sin\frac{\theta}{2}(\kappa - \sin\theta) + K_2^{\text{aux}} \cos\frac{\theta}{2}(\kappa - 2 + \cos\theta)\right\} \tag{A6}$$

$$u_3^{\text{aux}} = \frac{2}{\mu}\sqrt{\frac{r}{2\pi}} K_3^{\text{aux}} \sin\frac{\theta}{2} \tag{A7}$$

where $\mu = E/2(1+\nu)$ and $\kappa = 3 - 4\nu$. See Figure 18 for the nomenclature.

ACKNOWLEDGEMENTS

The support of the Office of Naval Research and Department of Energy to Northwestern University, is gratefully acknowledged as well as the French support from the Direction des Systèmes de Force et de la Prospective, Délégation Générale pour l'Armement. We are also grateful to Jean-Francois Remacle for his help in using the AOMD C++ library and to Natarajan Sukumar for his comments.

REFERENCES

1. Belytschko T, Black T. Elastic crack growth in finite elements with minimal remeshing. *International Journal for Numerical Methods in Engineering* 1999; **45**(5):601–620.
2. Moës N, Dolbow J, Belytschko T. A finite element method for crack growth without remeshing. *International Journal for Numerical Methods in Engineering* 1999; **46**:131–150.
3. Dolbow J, Moës N, Belytschko T. Discontinuous enrichment in finite elements with a partition of unity method. *Finite Elements in Analysis and Design* 2000; **36**:235–260.
4. Melenk J, Babuška I. The partition of unity finite element method: Basic theory and applications. *Computer Methods in Applied Mechanics and Engineering* 1996; **39**:289–314.
5. Daux C, Moës N, Dolbow J, Sukumar N, Belytschko T. Arbitrary branched and intersecting cracks with the extended finite element method. *International Journal for Numerical Methods in Engineering* 2000; **48**: 1741–1760.
6. Belytschko T, Moës N, Usui S, Parimi C. Arbitrary discontinuities in finite elements. *International Journal for Numerical Methods in Engineering* 2001; **50**:993–1013.
7. Sukumar N, Chopp DL, Moës N, Belytschko T. Modeling holes and inclusions by level sets in the extended finite element method. *Computer Methods in Applied Mechanics and Engineering* 2001; **190**:6183–6200.
8. Stolarska M, Chopp DL, Moës N, Belytschko T. Modelling crack growth by level sets and the extended finite element method. *International Journal for Numerical Methods in Engineering* 2001; **51**(8):943–960.
9. Sukumar N, Moës N, Belytschko T, Moran B. Extended finite element method for three-dimensional crack modelling. *International Journal for Numerical Methods in Engineering* 2000; **48**(11):1549–1570.
10. Sukumar N, Chopp DL, Moran B. Extended finite element method and fast marching method for three-dimensional fatigue crack propagation. *Engineering Fracture Mechanics* 2001, submitted.
11. Carter B, Wawrzynek P, Ingraffea A. Automated 3d crack growth simulation. *International Journal for Numerical Methods in Engineering* 2000; **47**:229–253.
12. Neto JC, Wawrzynek P, Carvalho M, Martha L, Ingraffea A. An algorithm for three-dimensional mesh generation for arbitrary regions with cracks. *Engineering with Computers* 2001; **17**(2001):75–91.
13. Dhondt G. Automatic 3-d mode in crack propagation calculations with finite elements. *International Journal for Numerical Methods in Engineering* 1998; **41**(4):739–757.
14. Gerstle WH, Martha L, Ingraffea AR. Finite and boundary element modeling of crack propagation in two- and three-dimensions. *Engineering with Computers* 1987; **2**:167–183.
15. Nishioka T, Atluri S. Analytical solution for embedded cracks, and finite element alternating method for elliptical surface cracks, subjected to arbitrary loading. *Engineering Fracture Mechanics* 1983; **17**:247–268.
16. Duarte CA, Hamzeh ON, Liszka TJ, Tworzydlo WW. A generalized finite method for the simulation of three-dimensional dynamic crack propagation. *Computer Methods in Applied Mechanics and Engineering* 2001; **190**:2227–2262.
17. Krysl P, Belytschko T. Element free Galerkin method for dynamic propagation of arbitrary 3-d cracks. *International Journal for Numerical Methods in Engineering* 1999; **44**(6):767–800.
18. Bolzon G, Corigliano A. Finite elements with embedded displacement discontinuity: a generalized formulation. *International Journal for Numerical Methods in Engineering* 2001; **49**(10):1227–1266.
19. Jirasek T, Zimmermann T. Embedded crack model: Part I basic formulation. *International Journal for Numerical Methods in Engineering* 2001; **50**(6):1269–1290.
20. Remacle J-F, Karamete BK, Shephard M. Algorithm oriented mesh database. *Ninth International Meshing Roundtable*, Sandia National Laboratories, pp. 349–359, October 2000.
21. Remacle J-F, Klaas O, Flaherty J, Shephard M. Parallel algorithm oriented mesh database. *Tenth International Meshing Roundtable*, Newport Beach, California, October 2001.
22. Moran B, Shih C. Crack tip and associated domain integrals from momentum and energy balance. *Engineering Fracture Mechanics* 1987; **127**:615–642.
23. Gosz M, Dolbow J, Moran B. Domain integral formulation for stress intensity factor computation along curved three-dimensional interface cracks. *International Journal of Solids and Structures* 1998; **35**:1763–1783.
24. Gosz M, Moran B. An interaction energy integral method for the computation of mixed-mode stress intensity factors along non-planar crack fronts in three dimensions. *Engineering Fracture Mechanics* 2001, to appear.
25. Destuynder P, Djaoua M, Lescure S. Some remarks on elastic fracture mechanics (quelques remarques sur la mécanique de la rupture élastique). *Journal de Mécanique théorique et appliquée* 1983; **2**(1):113–135.

26. Belytschko T, Liu W, Moran B. *Nonlinear Finite Elements for Continua and Structures*. Wiley: New York, 2000.
27. Gravouil A, Moës N, Belytschko T. Non-planar 3D crack growth by the extended finite element and level sets. Part II: level set update. *International Journal for Numerical Methods in Engineering* 2002; **53**:2569–2586.
28. Martynenko M, Ulitko A. Stress state near the vertex of a spherical notch in an unbounded elastic medium. *Soviet Applied Mechanics* 1978; **14**(2):15–23.
29. Singh R, Carter B, Wawrzynek P, Ingraffea A. Universal crack closure integral for sif estimation. *Engineering Fracture Mechanics* 1998; **60**(2):133–146.
30. Kassir M, Sih G. Three-dimensional stress distribution around an elliptical crack under arbitrary loadings. *IMA Journal of Applied Mathematics* 1966; **33**:601–611.
31. Remacle J-F, Geuzaine C. Gmsh finite element grid generator. Available at www.geuz.org/gmsh, 1998.